LETTER

doi:10.1038/nature12044

Mapping molecular motions leading to charge delocalization with ultrabright electrons

Meng Gao[1,2]*, Cheng Lu[1], Hubert Jean-Ruel[1,2], Lai Chung Liu[1,2], Alexander Marx[2], Ken Onda[3,4], Shin-ya Koshihara[5,6], Yoshiaki Nakano[7], Xiangfeng Shao[7]†, Takaaki Hiramatsu[8], Gunzi Saito[8], Hideki Yamochi[7], Ryan R. Cooney[1,2], Gustavo Moriena[1,2], Germán Sciaini[1,2]* & R. J. Dwayne Miller[1,2]

Ultrafast processes can now be studied with the combined atomic spatial resolution of diffraction methods and the temporal resolution of femtosecond optical spectroscopy by using femtosecond pulses of electrons[1–14] or hard X-rays[15–19] as structural probes. However, it is challenging to apply these methods to organic materials, which have weak scattering centres, thermal lability, and poor heat conduction. These characteristics mean that the source needs to be extremely bright to enable us to obtain high-quality diffraction data before cumulative heating effects from the laser excitation either degrade the sample or mask the structural dynamics[20]. Here we show that a recently developed, ultrabright femtosecond electron source[7–9] makes it possible to monitor the molecular motions in the organic salt (EDO-TTF)$_2$PF$_6$ as it undergoes its photo-induced insulator-to-metal phase transition[21–24]. After the ultrafast laser excitation, we record time-delayed diffraction patterns that allow us to identify hundreds of Bragg reflections with which to map the structural evolution of the system. The data and supporting model calculations indicate the formation of a transient intermediate structure in the early stage of charge delocalization (less than five picoseconds), and reveal that the molecular motions driving its formation are distinct from those that, assisted by thermal relaxation, convert the system into a metallic state on the hundred-picosecond timescale. These findings establish the potential of ultrabright femtosecond electron sources[7–14] for probing the primary processes governing structural dynamics with atomic resolution in labile systems relevant to chemistry and biology.

(EDO-TTF)$_2$PF$_6$ (where EDO-TTF is ethylenedioxytetrathiafulvalene) is a quasi-one-dimensional, 3/4-band-filled charge-transfer organic salt that undergoes a thermally induced insulator-to-metal phase transition at a critical temperature of $T_c \approx 280$ K (ref. 21) and also a highly efficient and ultrafast photo-induced phase transition[22–24]. Its electronic structure resembles that of Bechgaard salts, which provided the first organic superconductor, (TMTSF)$_2$PF$_6$ (see ref. 25). The origin of its insulator-to-metal phase transition involves a variety of collective phenomena[23]: Peierls-and-Holstein-type electron–phonon[26] and antiferromagnetic interactions[27], that coexist with order–disorder[21,24] charge localization, and long-range Coulombic interactions have an important role in charge disproportionation[28]. In its metallic or high-temperature (HT) phase, electron donor EDO-TTF molecules (D) form columns of cations that are separated by sheets of acceptor PF$_6$ anions. The distribution of positive charges among EDO-TTF molecules along the stacking direction is represented by ($D^{+0.5}D^{+0.5}D^{+0.5}D^{+0.5}$) as shown in Fig. 1 (top right)[21–24]. The high positive charge mobility along the cation stacks confers metallic properties at room temperature. The holes localize below T_c and endow the low-temperature (LT) phase with insulating properties. In the LT phase, the EDO-TTF molecules present a charge-ordered[21–24] state ($D^{+1}D^{+0}D^{+0}D^{+1}$), in which a large bending of the neutral moieties promotes the doubling of the unit cell akin to a Peierls mechanism in a half-band-filled system, as shown in Fig. 1 (top left). Model calculations predict that vertical photo-excitation via the second charge-transfer band[26] leads to a localized {$D^{+2}D^{+0}D^{+0}D^{+0}$} excited state. Time-resolved optical reflectivity measurements in combination with theoretical modelling indicate[23] that this initial excited state evolves in less than 100 fs into a ($D^{+1}D^{+0}D^{+1}D^{+0}$) charge-disproportionate state, which has a lifetime of about 4 ps. Time-resolved optical studies in the near- and mid-infrared region identify large charge fluctuations as the driving process that finally leads to the complete randomization and melting of the charge order after about 100 ps (ref. 24).

To probe the structural evolution in (EDO-TTF)$_2$PF$_6$ directly during its photo-induced insulator-to-metal phase transition, we performed femtosecond electron diffraction (FED) studies employing a recently developed ultrabright femtosecond electron source[7–9] that can

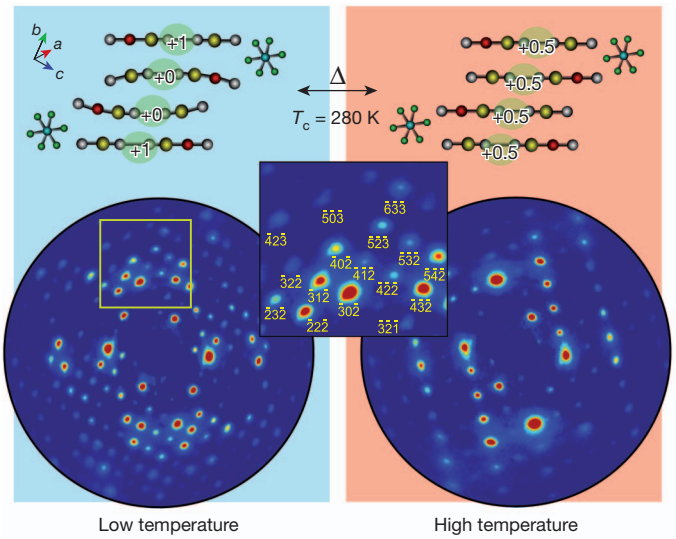

Figure 1 | Insulator-to-metal first-order phase transition in (EDO-TTF)$_2$PF$_6$. Top panels, illustration of the molecular and electronic changes associated with the thermal insulator-to-metal phase transition. Bottom panels, diffraction patterns for the LT and HT phases, obtained at 230 K and 295 K, respectively. The inset shows the assigned Miller indices (h, k, l). The symmetry breaking (cell doubling) corresponds to peaks indexed with $k = 2n + 1$ in the LT phase. For details about the definition of unit cell axes, see Supplementary Information section 6.1.

[1]Departments of Chemistry and Physics, University of Toronto, Toronto, Ontario M5S 3H6, Canada. [2]Max Planck Research Department for Structural Dynamics, Department of Physics, University of Hamburg, Hamburg Center for Ultrafast Imaging, Luruper Chaussee 149, 22761 Hamburg, Germany. [3]Interactive Research Center of Science, Tokyo Institute of Technology, Nagatsuta, Midori-ku, Yokohama 226-8502, Japan. [4]PRESTO, Japan Science and Technology Agency, Honcho, Kawaguchi 332-0012, Japan. [5]Department of Chemistry and Materials Science, Tokyo Institute of Technology, Ōokayama, Meguro-ku, Tokyo 152-8551, Japan. [6]CREST, Japan Science and Technology Agency (JST), 5-3, Yonbancho, Chiyoda-ku, Tokyo 102-8666, Japan. [7]Research Center for Low Temperature and Materials Sciences, Kyoto University, Sakyo-ku, Kyoto 606-8501, Japan. [8]Faculty of Agriculture, Meijo University, Shiogamaguchi 1-501 Tempaku-ku, Nagoya 468-8502, Japan. †Present address: State Key Laboratory of Applied Organic Chemistry, Lanzhou University, 222 Tianshui South Road, Lanzhou 730000, Gansu, China.
*These authors contributed equally to this work.

deliver high-quality diffraction from low-atomic-number materials even at the very low repetition rate of only 10 Hz used to avoid the adverse effects caused by cumulative heating. FED experiments were performed in transmission mode, with the electron beam propagating nearly perpendicular to the stacking direction of the EDO-TTF moieties to ensure high sensitivity to the most relevant molecular motions, that is, those associated with the dynamics of the EDO-TTF moieties and PF_6 counter-ions. Samples were kept at 230 K (for the LT phase) and photo-excited by 60-fs, 800-nm light while being monitored by ultrabright femtosecond electron pulses, with 200 or more reflections enabling us to track time-dependent changes beyond the noise level. See the Supplementary Information for detailed information about methodology (sections 1–3), sample preparation (section 5), sample orientation (sections 6.1 and 6.4), and control experiments (section 4).

Figure 1 depicts the molecular arrangement of EDO-TTF moieties with their respective charge distributions for the LT and HT phases, along with the corresponding electron diffraction patterns. The appearance of a new family of peaks in the diffraction pattern of the LT phase is indicative of a cell-doubling effect, with the clear difference between the diffraction patterns of the LT and HT phases confirming that the crystal orientation allows the observation of the relevant structural changes.

We monitor the structural evolution of the system by collecting diffraction patterns at different time delays after photoexcitation and using the pattern of the initial LT phase as a reference, with the resulting difference patterns shown in Fig. 2a. For comparison, Fig. 2b shows the difference between the diffraction patterns of the HT and LT phases (shown in Fig. 1). Figure 2c gives the temporal evolution of normalized intensity changes for some selected Bragg reflections, which allow separation of the observed photo-induced structural dynamics into a 'fast' component in the subpicosecond-to-picosecond range and a 'slow' structural change proceeding on the 100-ps timescale. The fast dynamics can be explained as femtosecond optical excitation altering the charge distribution, modifying the inter- and intramolecular forces and driving coherent molecular motions. The slow dynamics are attributed to uncorrelated motions that provide an ensemble-averaged picture of the structural evolution, that is, a thermal relaxation process that brings the system to a metallic HT-type state[24]. The transfer of heat to the lattice manifests itself as slow oscillations of diffracted intensities (see right panel in Fig. 2c) which are probably introduced through the generation of strain waves[29]. The most noteworthy feature is the plateau behaviour observed for time delays from about 3 ps to 10 ps (left panel of Fig. 2c), which reflects a transient intermediate structure (TIS). Given that optical studies indicate large charge fluctuations[23] prevailing in this time span[24], it seems plausible that the effective intermolecular forces are screened and the structure therefore transiently locked.

To obtain a time-dependent map of the relevant molecular motions driving the insulator-to-metal phase transition and the formation of the TIS, we developed a structural refinement algorithm based on a parameterized molecular model (see equations (4), (6), (7) and (8) in Supplementary Information section 7). The model makes use of the LT and HT structures as previously determined by X-ray diffraction[21] and considers about 40 Bragg reflections in the refinement calculations. The selection of reflections was based on their proximity to the Ewald sphere (Bragg condition) and the necessity of removing overlapped peaks.

The entire data set of diffraction images was reduced to the square root of intensities, that is, structure factor amplitudes $|F_{exp}(k, t)|$ (besides a k-dependent constant), where k denotes the scattering vector (or Miller indices) and t is a given time delay. Given that optical excitation causes only a small fraction of unit cells (η_{exc}) to undergo

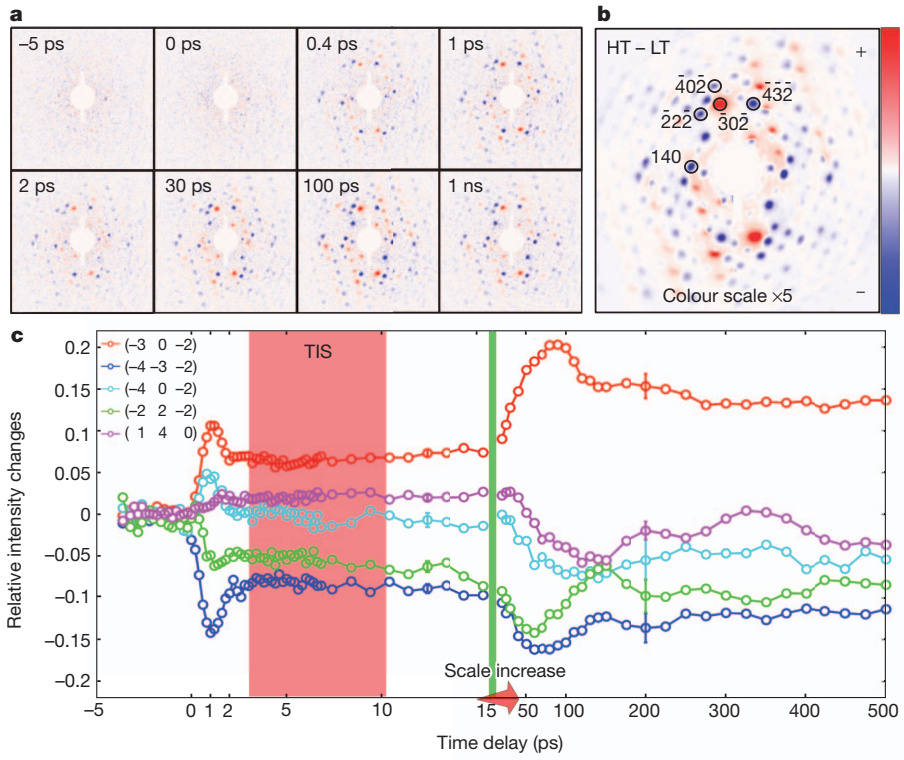

Figure 2 | Photo-induced time-dependent structural changes monitored by ultrabright FED. a, Differences between the diffraction patterns of the photo-induced and the initial LT phases as a function of the time delay between the optical excitation and electron probe pulses. **b**, Difference between the diffraction patterns of the HT and LT phases (shown in Fig. 1). **c**, Relative intensity changes for a few selected reflections. On the left side of the vertical green line, fast dynamical processes are shown; on the right side, slow dynamical processes are shown. The excitation fluence was 0.55 mJ cm^{-2}. The sample was photo-excited by 60-fs, 800-nm optical pulses at a repetition rate of 10 Hz. Error bars represent the standard deviation of measured values within the set of ten identical trials.

structural changes (see Supplementary Figs 9, 12 and 15), the observed experimental structure factor amplitudes can be written[30] as $|F_{exp}(k, t)| = |\eta_{exc}F_{exc}(k, t) + (1 - \eta_{exc})F_{LT}(k)|$, where $F_{exc}(k, t)$ is the relevant part showing time-dependent changes and $F_{LT}(k)$ are the structure factor amplitudes of the initial LT phase. The structure factor amplitudes are weighted by the fraction of unit cells being altered, and remaining in the LT phase, respectively. Our model refinement calculations compare $|F_{exp}(k, t)|$ with simulated amplitudes $|F_{sim}(k, \xi)| = |\eta_{exc}F_{sim,\,exc}(k, \xi) + (1 - \eta_{exc})F_{sim,\,LT}(k)|$ and maximize the Pearson correlation coefficient, $\gamma(|F_{exp}|, |F_{sim}|)$. This figure of merit γ varies between 0 (no correlation) and 1 (full correlation) and was found to provide well-behaved maxima across the full time series (see Supplementary Figs 14 and 15).

The term ξ is an atomic structural parameter composed of the three time-dependent generalized reaction coordinates (ξ_F, ξ_B, ξ_P) assigned to the motion of three independent dynamic groups: flat EDO-TTF molecules, bent EDO-TTF moieties and PF_6 anions, respectively. The configuration space was created from a linear interpolation (for each dynamic group) between the initial $\{\xi = (0, 0, 0)\}$ LT and the final $\{\xi = (1, 1, 1)\}$ HT-type structures (see Supplementary Table 2). We believe that the reduction of the problem to such reaction coordinates (see Fig. 3a) should capture most of the physics and, at the same time, avoid unphysical results as a consequence of over-fitting. A value of $\eta_{exc} \approx 0.1$ was obtained by maximizing $\gamma(\eta_{exc})$ in the time interval of 0–10 ps (see Supplementary Fig. 15) and found to be in very good agreement with the estimated number of converted unit cells into the HT-type state obtained from equation (5) of the Supplementary Information and from the decrease at $t = 1$ ns in the structure factor amplitude averaged over $(h, k = 2n + 1, l)$-reflections (where n is an integer) shown in Supplementary Fig. 9. Such reflections disappear in the HT phase owing to its higher symmetry (see Supplementary Information section 6.2).

These last two estimations of η_{exc} rely on the fact that by $t = 1$ ns the system has fully thermalized in a HT-type state and little residual thermal stress is left. These are fair assumptions considering that for $t > 500$ ps, the oscillations are damped, the estimated temperature increase is less than 50 K and the effect of residual stress is minimized for reflections satisfying Bragg's law[29]. From optical reflectivity and

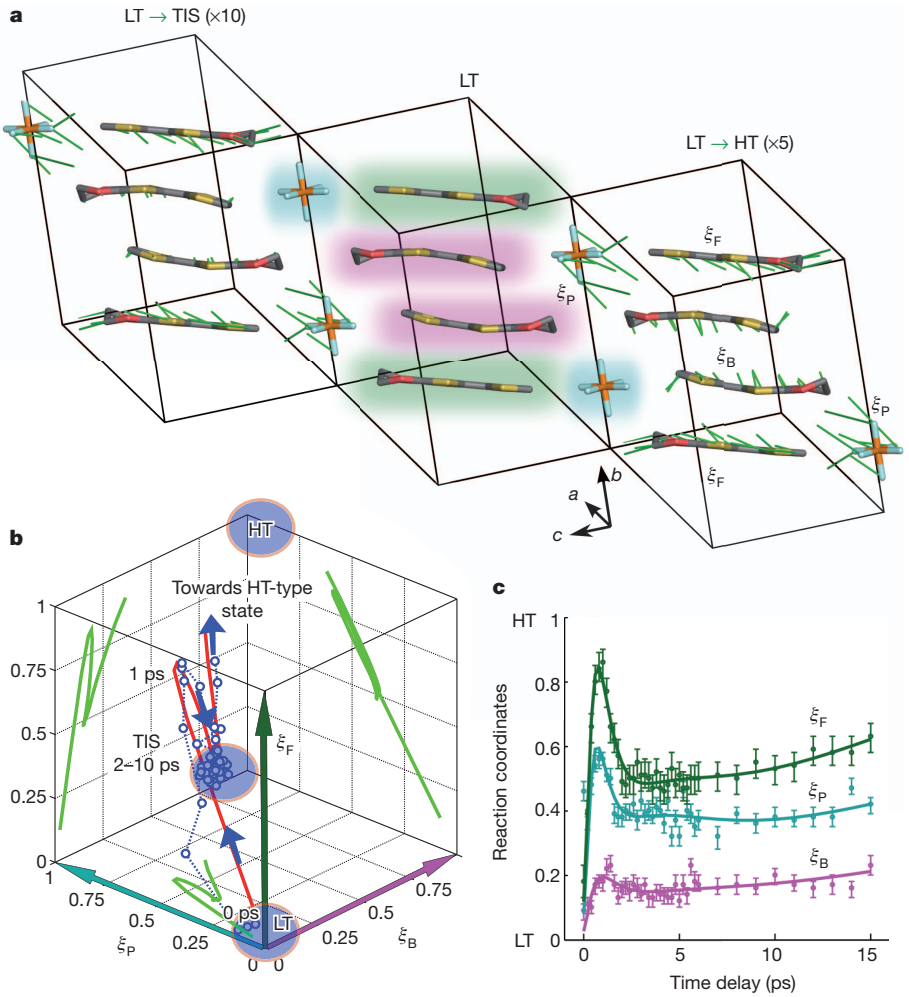

Figure 3 | Reaction coordinates and their temporal evolution in the formation of TIS. a, Three unit cells illustrating the arrangement of EDO-TTF molecules and PF_6 counter-ions in the LT phase. Selected dynamical groups are illustrated using different background colours in the central unit cell: flat EDO-TTF moieties have a green background, bent EDO-TTF moieties have a pink background, and PF_6 anions have a cyan background. Green sticks denote the atomic displacements from the initial LT structure to the TIS (unit cell on the left) and the HT-type structure (unit cell on the right); displacements were magnified 10 and 5 times, respectively, for clarity. The root-mean-square displacement between the LT structure and the TIS is 0.18 Å and between the LT and HT-type structures is 0.44 Å. The atomic coordinates of the TIS are listed in Supplementary Table 2. **b**, Temporal evolution of ξ in a (ξ_F, ξ_B, ξ_P)-Cartesian configuration space. Circles indicate optimized structures. The red trace is a multi-exponential fit of the optimum correlation trajectory. The green trajectories are two-dimensional projections. **c**, Temporal evolution of each reaction coordinate and its contribution in the formation of the TIS. Error bars represent the full-width at half-maximum (FWHM) of the global maximum peaks of the Pearson correlation coefficient in reaction coordinate space. Solid traces are multi-exponential fits; see equation (9) in the Supplementary Information and Supplementary Table 1. See Supplementary Videos for full molecular movies highlighting the key molecular motions leading to the formation of the TIS state.

in situ transmission measurements we estimated that, for the excitation level used in the experiments, about 8% of the LT unit cells are initially photo-excited (see Supplementary Information section 2). The above observations indicate that the initial excitonic correlation length only extends over about one LT unit cell, promoting local structural changes.

Figure 3a depicts the selected dynamical groups (central unit cell) and the atomic displacements connecting the LT structure with the TIS (on the left) and the HT-type structures (on the right), respectively. The root-mean-square displacement between the LT structure and the TIS is 0.18 Å and between the LT and HT structures is 0.44 Å. Figure 3b summarizes the time-dependent changes of ξ, illustrated in a (ξ_F, ξ_B, ξ_P)-Cartesian configuration space. As can be seen from the two-dimensional projections, the motions of flat EDO-TTF moieties and of PF_6 counter-ions are correlated. The temporal evolution of each reaction coordinate is also shown in Fig. 3c, for clearness. The relative values among reaction coordinates suggest that optical excitation mostly drives the formation of the TIS through the sliding of flat EDO-TTF moieties and the correlated motion of PF_6 counter-ions. This observation is also supported by their respective overshoot values, $\Delta \equiv \xi(1\,\mathrm{ps}) - \xi(5\,\mathrm{ps})$, which are indicative of an over-damped half-cycle motion. The close proximity of PF_6 anions to EDO-TTF molecules and the observed correlation suggest that steric effects—that is, short-range repulsive interactions— are also important in the crystalline order and positioning of the anions.

The addition of nearest-neighbour Coulomb repulsion and electron–phonon interactions that modulate site energies through anion displacements were found to be crucial to reproduce the spectral signature of the $(D^{+1}D^{+0}D^{+1}D^{+0})$ excited state via an extended Peierls–Holstein–Hubbard model[23]. Our results correspondingly indicate the motion of PF_6 counter-ions as a relevant component of the structural evolution of the excited electronic state and the formation of the TIS. Their connection with charge fluctuations suggests that PF_6 counter-ions need to be modified in order to gain control over electronic properties in $(EDO\text{-}TTF)_2PF_6$, akin to the anion replacement that confers superconductive properties at ambient pressure when going from $(TMTSF)_2PF_6$ to $(TMTSF)_2ClO_4$ (ref. 25). In contrast, the small relative amplitude for the unbending of EDO-TTF molecules in the formation of the TIS questions the relevance of this simple bending-type distortion mode in the formation of its charge disproportionates. Future FED experiments will focus on different sample orientations with improved spatial resolution and apply more general refinement algorithms for real-space reconstruction and *ab initio* electronic calculations to link dynamical structures with time-evolving charge distributions.

Received 10 August 2012; accepted 20 February 2013.

1. Sciaini, G. & Miller, R. J. D. Femtosecond electron diffraction: heralding the era of atomically-resolved dynamics. *Rep. Prog. Phys.* **74,** 096101 (2011).
2. Siwick, B. J., Dwyer, J. R., Jordan, R. E. & Miller, R. J. D. An atomic-level view of melting using femtosecond electron diffraction. *Science* **302,** 1382–1385 (2003).
3. Chergui, M. & Zewail, A. H. Electron and X-ray methods of ultrafast structural dynamics: advances and applications. *Phys. Chem. Chem. Phys.* **10,** 28–43 (2009).
4. Baum, P. & Zewail, A. H. Breaking resolution limits in ultrafast electron diffraction and microscopy. *Proc. Natl Acad. Sci. USA* **103,** 16105–16110 (2006).
5. Raman, R. K. *et al.* Direct observation of optically induced transient structures in graphite using ultrafast electron crystallography. *Phys. Rev. Lett.* **101,** 077401 (2008).
6. Eichberger, M. *et al.* Snapshots of cooperative atomic motions in the optical suppression of charge density waves. *Nature* **468,** 799–802 (2010).
7. Van Oudheusden, T. *et al.* Compression of subrelativistic space-charge-dominated electron bunches for single-shot femtosecond electron diffraction. *Phys. Rev. Lett.* **105,** 264801 (2010).
8. Gao, M. *et al.* Full characterization of RF compressed femtosecond electron pulses using ponderomotive scattering. *Opt. Express* **20,** 12048–12058 (2012).
9. Chatelain, R. P., Morrison, V. R., Godbout, C. & Siwick, B. J. Ultrafast electron diffraction with radio-frequency compressed electron pulses. *Appl. Phys. Lett.* **101,** 081901 (2012).
10. Hastings, J. B. *et al.* Ultrafast time-resolved electron diffraction with megavolt electron beams. *Appl. Phys. Lett.* **89,** 184109 (2006).
11. Musumeci, P., Moody, J. T., Scoby, C. M., Gutierrez, M. S. & Westfall, M. Laser-induced melting of a single crystal gold sample by time-resolved ultrafast relativistic electron diffraction. *Appl. Phys. Lett.* **97,** 063502 (2010).
12. Tokita, S. *et al.* Single-shot femtosecond electron diffraction with laser-accelerated electrons: experimental demonstration of electron pulse compression. *Phys. Rev. Lett.* **105,** 215004 (2010).
13. Murooka, Y. *et al.* Transmission-electron diffraction by MeV electron pulses. *Appl. Phys. Lett.* **98,** 251903 (2011).
14. Kassier, G. H. *et al.* Photo-triggered pulsed cavity compressor for bright electron bunches in ultrafast electron diffraction. *Appl. Phys. B* **109,** 249–257 (2012).
15. Rousse, A. *et al.* Non-thermal melting in semiconductors measured at femtosecond resolution. *Nature* **410,** 65–68 (2001).
16. Sokolowski-Tinten, K. *et al.* Femtosecond X-ray measurement of coherent lattice vibrations near the Lindemann stability limit. *Nature* **422,** 287–289 (2003).
17. Zamponi, F., Rothhardt, P., Stingl, J., Woerner, M. & Elsaesser, T. Ultrafast large-amplitude relocation of electronic charge in ionic crystals. *Proc. Natl Acad. Sci. USA* **109,** 5207–5212 (2012).
18. Fritz, D. M. *et al.* Ultrafast bond softening in bismuth: mapping a solid's interatomic potential with X-rays. *Science* **315,** 633–636 (2007).
19. Beaud, P. *et al.* Spatiotemporal stability of a femtosecond hard–X-ray undulator source studied by control of coherent optical phonons. *Phys. Rev. Lett.* **99,** 174801 (2007).
20. Poulin, P. R. & Nelson, K. A. Irreversible organic crystalline chemistry monitored in real time. *Science* **313,** 1756–1760 (2006).
21. Ota, A., Yamochi, H. & Saito, G. A novel metal-insulator phase transition observed in $(EDO\text{-}TTF)_2PF_6$. *J. Mater. Chem.* **12,** 2600–2602 (2002).
22. Chollet, M. *et al.* Gigantic photoresponse in 1/4-filled-band organic salt $(EDO\text{-}TTF)_2PF_6$. *Science* **307,** 86–89 (2005).
23. Onda, K. *et al.* Photoinduced change in the charge order pattern in the quarter-filled organic conductor $(EDO\text{-}TTF)_2PF_6$ with a strong electron-phonon interaction. *Phys. Rev. Lett.* **101,** 067403 (2008).
24. Fukazawa, N. *et al.* Charge and structural dynamics in photoinduced phase transition of $(EDO\text{-}TTF)_2PF_6$ examined by picosecond time-resolved vibrational spectroscopy. *J. Phys. Chem. C* **116,** 5892–5899 (2012).
25. Jérôme, D. The physics of organic superconductors. *Science* **252,** 1509–1514 (1991).
26. Yonemitsu, K. & Maeshima, N. Photoinduced melting of charge order in a quarter-filled electron system coupled with different types of phonons. *Phys. Rev. B* **76,** 075105 (2007).
27. Filatov, M. Antiferromagnetic interactions in the quarter-filled organic conductor $(EDO\text{-}TTF)_2PF_6$. *Phys. Chem. Chem. Phys.* **13,** 12328–12334 (2011).
28. Iwano, K. & Shimoi, Y. Large electric-potential bias in an EDO-TTF tetramer as a major mechanism of charge ordering observed in its PF_6 salt: a density functional theory study. *Phys. Rev. B* **77,** 075120 (2008).
29. Harb, M. *et al.* Excitation of longitudinal and transverse coherent acoustic phonons in nanometer free-standing films of (001) Si. *Phys. Rev. B* **79,** 094301 (2009).
30. Coppens, P., Vorontsov, I. I., Graber, T., Gembicky, M. & Kovalevsky, A. Y. The structure of short-lived excited states of molecular complexes by time-resolved X-ray diffraction. *Acta Crystallogr. A* **61,** 162–172 (2005).

Supplementary Information is available in the online version of the paper.

Acknowledgements We acknowledge the contributions of J. Stampe, M. de Jong, M. Harb and S. G. Kruglik in developing the radio-frequency cavity system and of E. Pelletier in developing the laser system. We also thank K. Iwano and M. Hoshino and K. Yonemitsu for discussions. Funding for this project was provided by the Natural Sciences and Engineering Research Council of Canada and the Canada Foundation for Innovation. This work was supported in part by a Grant-in-Aid for Scientific Research on Innovative Areas (grant number 20110006) and the Global Centre of Excellence (G-COE) programme for Chemistry from The Ministry of Education, Culture, Sports, Science and Technology in Japan and by Creative Scientific Research (grant number 18GS0208) from The Japan Society for the Promotion of Science.

Author Contributions FED experiments were performed at University of Toronto in R.J.D.M.'s group. G. Sciaini initiated the EDO studies and conducted the work with R.J.D.M. C.L., G.M. and G. Sciaini performed the initial FED experiments at 1 kHz and 100 Hz. M.G., H.J.-R. and R.R.C. performed the final FED experiments with ultrabright electron pulses. M.G., H.J.-R., L.C.L. and A.M. did the data analysis. L.C.L. did the model structural refinement calculations and the Supplementary Video. M.G., H.J.-R. and R.R.C. performed the optical transmission measurements. K.O. and S.-y.K. performed the optical reflectivity measurements. Y.N., X.S., T.H., G. Saito and H.Y. provided the single crystals. C.L. was responsible for sample preparation for FED. M.G., L.C.L. and A.M. wrote the Supplementary Information. G. Sciaini, C.L., M.G. and R.J.D.M. wrote the manuscript with discussions among all authors.

Author Information Reprints and permissions information is available at www.nature.com/reprints. The authors declare no competing financial interests. Readers are welcome to comment on the online version of the paper. Correspondence and requests for materials should be addressed to R.J.D.M. (dwayne.miller@mpsd.cfel.de).